

Degradation Process of Lead Chromate in Paintings by Vincent van Gogh Studied by Means of Synchrotron X-ray Spectromicroscopy and Related Methods. 1. Artificially Aged Model Samples

Letizia Monico,^{†,§} Geert Van der Snickt,[§] Koen Janssens,^{*,§} Wout De Nolf,[§] Costanza Miliani,[‡] Johan Verbeeck,[†] He Tian,[†] Haiyan Tan,[†] Joris Dik,[¶] Marie Radepont,^{§,△} and Marine Cotte^{△,▲}

[†]Dipartimento di Chimica and [‡]CNR di Scienze e Tecnologie Molecolari (CNR-ISTM), Università degli Studi di Perugia, via Elce di Sotto 8, I-06123 Perugia, Italy

[§]Department of Chemistry, University of Antwerp, Universiteitsplein 1, B-2610 Wilrijk, Belgium

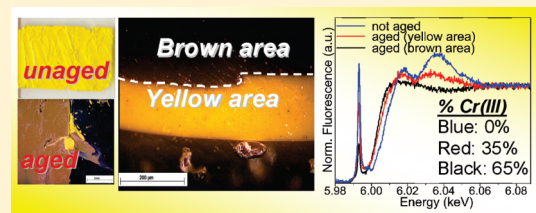
[†]Department of Physics, Electron Microscopy For Materials Science (EMAT), University of Antwerp, Groenenborgerlaan 171, B-2020 Antwerp, Belgium

[¶]Department of Materials Science and Engineering, Delft University of Technology, Mekelweg 2, NL-2628CD Delft, The Netherlands

[△]Centre de Recherche et de Restauration des Musées de France, CNRS UMR171, Palais du Louvre, Porte des Lions, 14 Quai François Mitterrand, F-75001 Paris, France

[▲]European Synchrotron Radiation Facility, Polygone Scientifique Louis Néel -6, rue Jules Horowitz — F-38000 Grenoble, France

ABSTRACT: On several paintings by artists of the end of the 19th century and the beginning of the 20th Century a darkening of the original yellow areas, painted with the chrome yellow pigment (PbCrO_4 , $\text{PbCrO}_4 \cdot x\text{PbSO}_4$, or $\text{PbCrO}_4 \cdot x\text{PbO}$) is observed. The most famous of these are the various *Sunflowers* paintings Vincent van Gogh made during his career. In the first part of this work, we attempt to elucidate the degradation process of chrome yellow by studying artificially aged model samples. In view of the very thin (1–3 μm) alteration layers that are formed, high lateral resolution spectroscopic methods such as microscopic X-ray absorption near edge (μ -XANES), X-ray fluorescence spectrometry (μ -XRF), and electron energy loss spectrometry (EELS) were employed. Some of these use synchrotron radiation (SR). Additionally, microscopic SR X-ray diffraction (SR μ -XRD), μ -Raman, and mid-FTIR spectroscopy were employed to completely characterize the samples. The formation of Cr(III) compounds at the surface of the chrome yellow paint layers is particularly observed in one aged model sample taken from a historic paint tube (ca. 1914). About two-thirds of the chromium that is present at the surface has reduced from the hexavalent to the trivalent state. The EELS and μ -XANES spectra are consistent with the presence of $\text{Cr}_2\text{O}_3 \cdot 2\text{H}_2\text{O}$ (viridian). Moreover, as demonstrated by μ -XANES, the presence of another Cr(III) compound, such as either $\text{Cr}_2(\text{SO}_4)_3 \cdot \text{H}_2\text{O}$ or $(\text{CH}_3\text{CO}_2)_7\text{Cr}_3(\text{OH})_2$ [chromium(III) acetate hydroxide], is likely.



Recent years have seen a growing interest in paintings of the end of the 19th Century and the beginning of the 20th Century from the field of analytical chemistry dedicated to the conservation of works of art. Since the beginning of 19th Century, the industrial expansion has stimulated the development of synthetic pathways for many new materials, including various pigments such as chrome yellow, cadmium yellow (CdS), emerald green [$\text{Cu}(\text{C}_2\text{H}_3\text{O}_2)_2 \cdot 3\text{Cu}(\text{AsO}_2)_2$], viridian green ($\text{Cr}_2\text{O}_3 \cdot 2\text{H}_2\text{O}$), and lithopone white ($\text{BaSO}_4 \cdot \text{ZnS}$). These new pigments were either synthetic, purer equivalents of the traditional pigments employed by painters in earlier periods or entirely new compounds, yielding brighter colors and providing new stylistic possibilities. Among these, chrome yellow pigments took an important position, outclassing, because of their brightness and opacity, the already existing yellow pigments [such as Naples yellow ($\text{Pb}_2\text{Sb}_2\text{O}_7$), orpiment (As_2S_3), yellow ochre (a mixture of iron oxides and hydroxides), etc.]. Chrome yellow, often encountered in paintings of the end of 19th Century, such as

by V. van Gogh (1853–1890),¹ G. Seurat (1859–1891),² J. M. W. Turner (1775–1851),³ J. Constable (1776–1837),⁴ P. Cézanne (1839–1906),⁵ C. Pissarro (1830–1903),⁶ and J. Ensor (1860–1949),⁷ is also employed on a wider scale for industrial purposes (painting of vehicles and air planes, road paint, and signs).

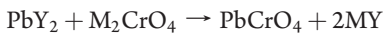
Chrome yellow belongs to a class of pigments based on either lead chromate (PbCrO_4 , yellow and found in nature as the rare mineral crocoite), lead chromate–oxide [$\text{PbCrO}_4 \cdot x\text{PbO}$, yellow-orange and found in nature as the mineral phoenicochroite with structure $\text{Pb}_2\text{O}(\text{CrO}_4)$], in which the lead oxide conveys a reddish shade, or lead chromate sulfate ($\text{PbCrO}_4 \cdot x\text{PbSO}_4$), in which the sulfate compounds are employed to obtain paler shades of yellow.^{8,9} At room temperature, PbCrO_4 and PbSO_4 , respectively, have a monoclinic and orthorhombic structure as

Received: September 22, 2010

Accepted: December 15, 2010

their most stable crystalline forms. When the relative atomic percentage of sulfate exceeds 40% in $\text{PbCrO}_4 \cdot x\text{PbSO}_4$, a change from the monoclinic to the orthorhombic structure is observed.^{10,11} Given its high cost, PbCrO_4 was often extended with various white compounds, e.g., with sulfates [BaSO_4 , $\text{CaSO}_4 \cdot 2\text{H}_2\text{O}$, $\text{KAl}(\text{SO}_4)_2 \cdot 12\text{H}_2\text{O}$, PbSO_4], with talc, calcite, or kaolin, or with other chromium-based yellow pigments such as CaCrO_4 and BaCrO_4 .⁹

The synthesis of chrome yellow has evolved over the years, since it was observed that its stability is related to the preparation procedure^{10,12} and to the presence of other species, such as organic compounds, or copper, phosphate, or chloride ions,¹⁰ or semiconductors particles, such as ZnO .¹⁷ In order to improve the light-fastness of PbCrO_4 , the initial custom of using lead acetate as one of the starting reagents was replaced by the use of neutral solutions/suspensions of a soluble lead salt, (e.g., lead nitrate, lead chloride) as reaction partner for alkaline (di)chromate solutions [usually K- or Na-(di)chromate],^{8,11} according to the reaction:



where $\text{M} = \text{Na}^+, \text{K}^+$ and $\text{Y} = \text{CH}_3\text{COO}^-, \text{NO}_3^-, \text{Cl}^-$, etc.

In the following years improvements in the stability of the pigment were obtained by treating it with a hydrous oxide of group IV or V metals.¹² Alternatively, PbCrO_4 can be synthesized through the direct addition of PbO to chromates in paste form.⁸

In some paintings by artists of the end of 19th Century such as Vincent van Gogh, more than one Century after their creation, the areas painted with chrome yellow now appear darkened, likely because of degradation of the pigment itself. Because of its instability, the painters of the 1880s gradually abandoned the use of chrome yellow,¹ replacing it by other pigments such as cadmium yellow, which was believed to be more stable.⁷ Recently, however, it was established that cadmium yellow can also become unstable,^{13,14} being oxidized from the yellow and opaque CdS to the white/transparent $\text{CdSO}_4 \cdot \text{H}_2\text{O}$.

The darkening of chrome yellow is reported as early as 1829,¹⁵ when it was observed that the pigment is subject to alteration when it is combined with oil, with lead oxide, or with Prussian blue. Nevertheless, it was not until the 20th Century that the degradation phenomenon of chrome yellow was systematically studied. Several studies on PbCrO_4 alteration, induced by the single or composite use of UV-visible light, heat, contaminants,^{10,11,16,17} and atmospheric gases, such as SO_2 ¹⁸ and H_2S ,¹⁹ are in agreement to attribute this degradation phenomenon to a reduction reaction of Cr(VI) to Cr(III); however, this assumption was not based on experimental evidence, nor was insight provided into the degradation mechanism or detailed information given about the nature of the degradation products. In this regard, some authors have proposed that the PbCrO_4 could dissociate by a photochemical reduction, into lead metachromite [$\text{Pb}(\text{CrO}_2)_2$], oxygen, and elementary lead,^{11,20} or into chrome oxide whereby Pb^{2+} is oxidized to PbO_2 .²¹ In the presence of SO_2 , under similar conditions, a mixture of PbSO_4 and Cr(III) compounds can be formed.¹⁸

After ca. 1950, the interest in the chrome yellow darkening problem diminished, probably because of the development of stabilized lead chromates and of more durable lead molybdates.^{8,10,18} However, in many scientific fields (e.g., in the environmental, industrial chemistry, biological, and geological areas) attempts have been made to better understand the reduction mechanism of Cr(VI). According to these recent literature data and consistent with the high oxidizing power of chromates, the reduction of Cr(VI) can be induced by many different agents, such as soil constituents

(e.g., amino, humic, and fulvic acids) and Fe(II),^{22,23} sulfides and sulfates,^{24,25} and organic matter,^{26,27} by semiconductors particles in aqueous solutions,^{28–30} or even by H_2O_2 in acidic aqueous solutions.^{31,32}

In recent years, various authors reconsidered the problem of the darkening of chromium-based yellow pigments ($\text{Pb}-, \text{Ba}-, \text{Sr}-, \text{Ca}-, \text{Zn}/\text{K-chromate}$) in the context of the conservation of paintings, because the understanding of the pigments' alteration process is of key importance both to adjust the conditions in which the works of art are stored and/or to allow the selection of an appropriate conservation treatment. Both studies that characterize several chromate samples taken from paints and paint tubes,³³ or that investigate which factors can promote the deterioration of zinc-potassium chromate,^{34,35} are reported in literature, showing that the alteration problem is not limited to PbCrO_4 alone. More specifically, in the recently published work by Casadio et al.,^{34,35} the discoloration of $\text{K}_2\text{O} \cdot 4\text{ZnCrO}_4 \cdot 3\text{H}_2\text{O}$ was attributed to the presence of Cr(VI) dichromate and of Cr(III) oxide species in the outer layers of model samples aged in a moist (90% relative humidity) SO_2 atmosphere. Also in historic samples from a painting by G. Seraut the ochre-colored discoloration of $\text{K}_2\text{O} \cdot 4\text{ZnCrO}_4 \cdot 3\text{H}_2\text{O}$ was found to be associated with both Cr(III) and Cr(VI) dichromate ions.

During the past decade, the introduction of synchrotron radiation-based methods of analysis in conservation science has led to increased insight into a number of alteration phenomena of different inorganic pigments.^{14,36–38} Especially, the ability of μ -XANES to visualize with micrometric resolution the distribution of specific species of a given chemical element is highly useful in this context. The capabilities of electron energy loss spectrometry (EELS) to render similar speciation information at the nanoscopic level is equally valuable, and both methods are used in a complementary fashion here.

In what follows, we attempt to elucidate the chemical transformations leading to the darkening of chrome yellow and to formulate hypotheses as to their cause. For this purpose, in the first part of this work, on the one hand μ -XANES and μ -XRF spectrometry and supporting analytical methods such as SR μ -XRD, Raman, and FTIR and on the other hand EELS spectroscopy were employed to study artificially aged model samples of lead chromate. The second part will focus on the study of two embedded paint cross-sections taken from paintings by Vincent van Gogh from the collection of the Van Gogh Museum (VGM), Amsterdam, where alteration of the chrome yellow is apparent.

■ EXPERIMENTAL SECTION

Materials. Aged Model Samples. Four model samples (A, B₁, B₂, C) were prepared for artificial aging by applying a thin layer of paint on glass microscopy slides (cf. Figure 2A). The paint layers were characterized before and after the aging process; some of their characteristics are summarized in Table 1. Model sample A was taken from a historic oil paint tube belonging to the Flemish Fauvist Rik Wouters (1882–1913); the tube was donated to the Royal Museum of Fine Arts of Antwerp after his death. Samples B₁ and B₂ similarly come from two different historic oil paint tubes of the end of 19th Century (Elsens, Bruxelles) provided by the Royal Academy of Fine Arts of Antwerp. As indicated by the labeling, the former is a light chrome yellow, while the latter is darker toned. Sample C was prepared in the laboratory by mixing pure PbCrO_4 with linseed oil (80:20 weight ratio). All the model samples were artificially

Table 1. Overview of Results of the Preliminary Characterization of the Unaged Model Samples

sample name	origin of paint	XRF	SR μ -XRD	μ -Raman	FTIR
A	historic oil paint tube belonging to the Flemish Fauvist Rik Wouters (1882–1913)	Pb, Cr	PbSO ₄ (anglesite) ^a	lead chromate, lead sulfate	lead chromate, lead sulfate
B ₁	historic end-19th century oil paint tube (Elsens, Bruxelles), light chrome yellow	Pb, Cr	PbCrO ₄ (crocoite)	lead chromate	lead chromate, lead sulfate
B ₂	historic end-19th Century oil paint tube (Elsens, Bruxelles), dark chrome yellow	Pb, Cr, Zn	PbCrO ₄ (crocoite), Pb ₂ O(CrO ₄) ₂ (phoenicochroite)	lead chromate (phoenicochroite)	lead chromate, lead sulfate
C	80:20 mixture of PbCrO ₄ powder with linseed oil	Pb, Cr	PbCrO ₄ (crocoite)	lead chromate	lead chromate

^a Because in sample A the presence of a crystalline form of PbCrO₄ could not be observed (next to that of well-crystallized PbSO₄) while on the other hand, the Raman, FTIR and XRF spectra are consistent with the presence of a major amount of PbCrO₄, we conclude that (most of) the PbCrO₄ in this oil paint is present in amorphous form.

186 aged for 800 h by means of SOLARBOX 1500e system (CO.FO.
187 ME.GRA., Milano, Italy), using a xenon UV lamp (irradiance 550
188 W/m²) at a temperature between 50 and 60 °C.

189 **Reference Compounds.** XANES spectra from the following
190 pure Cr-compounds were recorded: PbCrO₄, BaCrO₄, Na₂CrO₄,
191 Na₂CrO₄·4H₂O, K₂Cr₂O₇, Cr₂O₃, (CH₃CO₂)₇Cr₃(OH)₂, KCr-
192 (SO₄)₂·12H₂O, K₃Cr(C₂O₄)₃·3H₂O, CrCl₃·6H₂O, Cr₂(SO₄)₃·
193 H₂O, CrPO₄·H₂O, Cr(C₅H₇O₂)₃ (Sigma-Aldrich), K₂CrO₄,
194 CrO₃ (Merck), (NH₄)₂CrO₄ (Fluka), Cr(NO₃)₃·9H₂O (Chem-
195 Lab), ZnCrO₄, (NH₄)₂Cr₂O₇, CaCrO₄, MgCrO₄·H₂O, Na₂-
196 Cr₂O₇·2H₂O (Alfa-Aesar), Cr₂O₃·2H₂O (Winsor and Newton).
197 For this purpose, finely milled powders of these compounds were
198 dusted onto adhesive tape in a thin layer. In addition, EELS refer-
199 ence spectra of the compounds PbCrO₄, Cr₂O₃·2H₂O, and PbSO₄
200 were recorded.

201 **Methods.** After a preliminary characterization of the model
202 samples (via XRF, SR μ -XRD, μ -Raman, and mid-FTIR trans-
203 mission spectroscopy), high resolution SR μ -XRF maps were
204 collected to identify and better document the elemental compo-
205 sition of paint layers and establish the presence of optional
206 degradation products. Additionally, SR μ -XANES analyses at the
207 Cr K-edge were performed at different points of both the aged
208 and unaged model samples. The resulting spectral distributions
209 were compared to references in order to obtain information
210 about the Cr oxidation state. The XANES spectra were fitted as
211 linear combination of a limited set of Cr-reference compound
212 spectra in order to semiquantitatively determine the Cr-specia-
213 tion. To confirm the XANES findings and to establish with
214 greater confidence the nature of the Cr-containing degradation
215 products, EELS analyses at the nanoscopic level were carried out
216 on one of the aged model samples.

217 μ -XRD experiments were conducted at Beamline L of the
218 Hamburger Synchrotronstrahlungslabor (HASYLAB, Hamburg,
219 Germany).³⁹ A Si(111) double-crystal monochromator with an
220 energy bandwidth $\Delta E/E$ of about 0.02% produces a monochro-
221 matic beam of 25 keV that was focused on the sample by means of
222 a single-bounce elliptical capillary with a divergence of 2 to
223 2.5 mrad, obtaining a focal spot diameter of about 15 μ m. A 2k \times
224 2k Mar CCD 165 area detector (165 mm diameter, Marresearch
225 GmbH, Norderstedt, Germany) with 80 μ m pixel size, was
226 employed in transmission geometry to collect diffraction patterns.

227 The instrument used to carry out FTIR analysis consists of a
228 JASCO FTIR 4100 spectrometer, equipped with a ceramic light
229 source, Michelson interferometer, and a DLATGS detector. All
230 spectral measurements were acquired in transmittance mode, in
231 an energy range of 4000–400 cm⁻¹ and at a resolution of

232 2 cm⁻¹. The spectra were recorded using 200 scans; background
233 correction was performed by means of a spectrum collected from
234 a pressed potassium bromide pellet. All powdered samples were
235 prepared with finely ground KBr using a manual hydraulic press.

236 μ -Raman spectra were recorded using a JASCO Ventuno
237 double-grating spectrophotometer equipped with a charge-
238 coupled device (CCD) detector cooled to -50 °C and coupled
239 to an optical microscope (Olympus). Raman spectra were
240 excited using green radiation (532 nm) from an Nd:YAG laser.
241 The laser power used to irradiate the samples was kept between 1
242 and 2 mW; the exposure time varied between 10 and 20 s with
243 five accumulations. The spectral resolution was about 2 cm⁻¹.
244 Calibration of the spectrometer was performed using the Raman
245 lines of two standards: polystyrene and sulfur.

246 All samples were transported to and examined by means of
247 μ -XRF and μ -XANES at the European Synchrotron Radiation
248 Facility (ESRF, Grenoble, France) using beamline ID21. This
249 instrument operates in the primary energy range from 2.1 to
250 7.2 keV. A Si(220) fixed-exit double-crystal monochromator
251 was used to produce a highly monochromatic primary beam
252 ($\Delta E/E = 10^{-4}$).

253 μ -XRF and μ -XANES experiments were performed in vacuum
254 (10⁻⁶ mbar) to (i) minimize air absorption (which is significant
255 for light elements and for low-energy X-ray fluorescence lines),
256 (ii) avoid contributions to the spectral background due to
257 scattering in air, and (iii) prevent sample contamination. Either
258 a collimated beam of 0.2 mm diameter or a focused beam of ca.
259 0.95 \times 0.25 μ m² (horizontal \times vertical), obtained by means of a
260 Fresnel zone plate, was used for sample irradiation. During the
261 μ -XANES energy scans, the position of the primary beam was
262 maintained stable within 0.5 μ m. The procedure employed for
263 correction of the beam spot motion during energy scans is
264 explained elsewhere.⁴⁰ The μ -XRF signals were collected in the
265 horizontal plane and perpendicular to the primary beam by
266 means of an HPGe solid-state energy-dispersive detector. This
267 device is characterized by a resolution of 130 eV at 6 keV; the
268 detection limit for elements with atomic number between P and
269 Fe typically is around 10 ppm. The sample surface was oriented
270 vertically and at an angle of 60° relative to the incident beam.
271 Both the setup and the procedure for evaluation of XRF spectra
272 are described in greater detail elsewhere.⁴¹ During the μ -XRF
273 mapping experiments, the fluorescence signals were generated by
274 employing a monochromatic primary beam of fixed energy
275 (around 5.989 keV at the Cr K-edge). To compensate for
276 incident beam intensity variations, a normalization detector
277 (I_0) is located just upstream of the sample. The program PyMca

278 was used to fit the fluorescence spectra and separate the different
 279 elemental contributions. In the present context, it was in particular crucial to distinguish the partially overlapping Pb–M lines
 280 and S–K lines. This program was employed as a batch-fitting
 281 procedure on each pixel of two-dimensional (2D) maps.⁴²

282 μ -XANES spectra were acquired by scanning the primary
 283 energy around the Cr K-edge (5.96–6.09 keV) with a step size of
 284 0.2 eV. The energy calibration was performed using a metallic Cr
 285 foil. For all XANES spectra, the procedure of normalization was
 286 performed by means of ATHENA, a software program widely
 287 used for (E)XA(F)S data analysis. In particular, edge-step
 288 normalization of the data was performed by means of linear
 289 pre-edge subtraction and by regression of a quadratic polynomial
 290 beyond the edge.⁴³ The same software was also used to carry out
 291 a linear combinatorial fitting of XANES spectra of unknown
 292 mixtures of Cr-species against a library of XANES spectra of pure
 293 Cr-reference compounds. During this procedure, ATHENA
 294 attempts to find the best fit between the XANES spectra of the
 295 unknown mixtures using a large number of different combina-
 296 tions of the available reference spectra. Prior to the analysis of the
 297 samples, reference XANES spectra were acquired from pure
 298 compound powders by using a 200 μm diameter X-ray beam,
 299 recorded in an air environment and in transmission mode.

300 Conventional transmission electron microscopy (TEM) imag-
 301 ing and EELS studies were conducted using a JEOL 3000F
 302 TEM/STEM, equipped with a postcolumn GIF2000 detector.
 303 The TEM specimens were prepared by site-specific focused ion
 304 beam milling (FIB) using in situ lift-out in a FEI FIB/SEM
 305 xT Nova Nanolab 200. The FIB sample preparation method
 306 allows an optimal sample thickness and is capable of producing
 307 micrometer sized, electron transparent samples from well-defined
 308 areas.

■ RESULTS AND DISCUSSION

311 Before discussion of the results obtained from (un)aged
 312 model samples, it is useful to describe the features of the XANES
 313 and EELS spectra derived from a series of Cr-reference
 314 compounds. Both XANES and EELS are techniques that are sensitive
 315 to the local chemical environment of the Cr atom and to its
 316 surrounding atoms. Because chromium can be present in com-
 317 pounds with various coordination geometries, oxidation states,
 318 and molecular structures, these properties are to some extent
 319 reflected in the XANES (Figure 1) and EELS spectra (Figure 4).

320 **XANES K-Edge Spectra of Cr-Reference Compounds.** Re-
 321 ference spectra of Cr(VI) and Cr(III) compounds were recorded
 322 and are shown in Figure 1A and 1B, respectively. Generally, the
 323 intensity of the pre-edge peak is correlated to the number of
 324 electron vacancies in the 3d orbitals of the Cr atom,⁴⁴ so that the
 325 relative area of the pre-edge peak is proportional to the relative
 326 amount of Cr(VI) in a material.

327 For the Cr(VI) compounds (Figure 1A) having a tetrahedral
 328 coordination geometry, it is possible to observe a well-defined
 329 pre-edge peak around 5.993 keV for the Cr K-edge.⁴⁵ This peak
 330 corresponds to a bound-state 1s to 3d dipole-forbidden transi-
 331 tion. The presence of the pre-edge peak is related to the non-
 332 centrosymmetric nature of the tetrahedral structure that favors a
 333 strong hybridization of the Cr(3d) and O(2p) orbitals. In Cr(III)
 334 compounds, that commonly exist in a centrosymmetrical octa-
 335 hedral geometry, the pre-edge features have a low intensity. Two
 336 pre-edge peaks are present around 5.990 and 5.993 keV; these
 337 bands are assigned to 1s \rightarrow 3d(t_{2g}) and 1s \rightarrow 3d(e_g) electronic

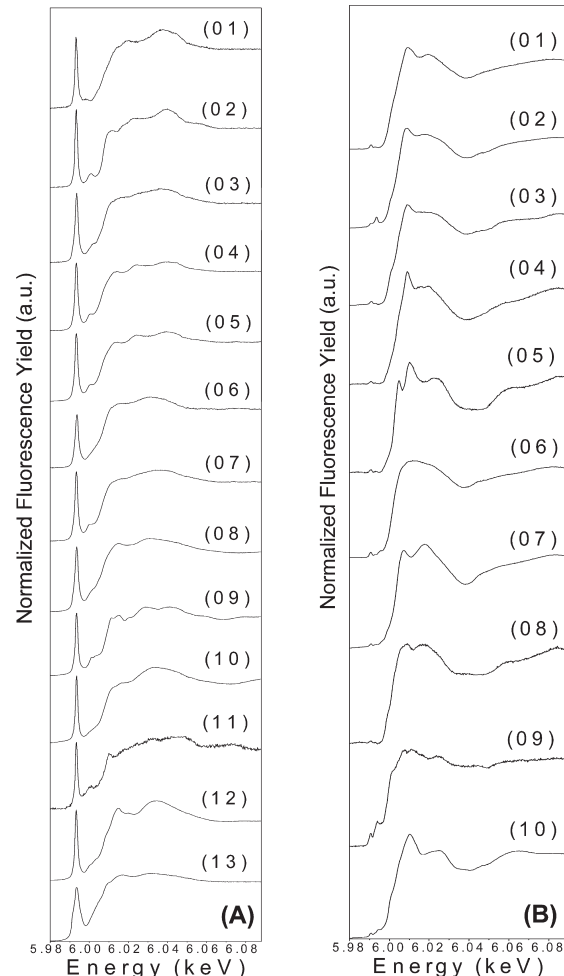


Figure 1. Cr K-edge μ -XANES spectra. Panel A: Cr(VI) reference compounds. (01) PbCrO_4 , (02) K_2CrO_4 , (03) $\text{K}_2\text{Cr}_2\text{O}_7$, (04) Na_2CrO_4 , (05) $\text{Na}_2\text{CrO}_4 \cdot 4\text{H}_2\text{O}$, (06) $\text{Na}_2\text{Cr}_2\text{O}_7 \cdot 2\text{H}_2\text{O}$, (07) $(\text{NH}_4)_2\text{CrO}_4$, (08) $(\text{NH}_4)_2\text{Cr}_2\text{O}_7$, (09) CaCrO_4 , (10) $\text{MgCrO}_4 \cdot \text{H}_2\text{O}$, (11) BaCrO_4 , (12) ZnCrO_4 , (13) CrO_3 . Panel B: Cr(III) reference compounds. (01) $\text{Cr}(\text{NO}_3)_3 \cdot 9\text{H}_2\text{O}$, (02) $\text{CrPO}_4 \cdot \text{H}_2\text{O}$, (03) $\text{Cr}_2(\text{SO}_4)_3 \cdot \text{H}_2\text{O}$, (04) $\text{KCr}(\text{SO}_4)_2 \cdot 12\text{H}_2\text{O}$, (05) $\text{K}_3\text{Cr}(\text{C}_2\text{O}_4)_3 \cdot 3\text{H}_2\text{O}$ (oxalate), (06) $(\text{CH}_3\text{CO}_2)_7\text{Cr}_3(\text{OH})_2$ (acetate), (07) $\text{Cr}(\text{C}_5\text{H}_7\text{O}_2)_3$ (acetylacetone), (08) $\text{CrCl}_3 \cdot 6\text{H}_2\text{O}$, (09) Cr_2O_3 , (10) $\text{Cr}_2\text{O}_3 \cdot 2\text{H}_2\text{O}$.

338 transitions, respectively. In addition, for Cr(VI) compounds, on
 339 the rising flank of the absorption edge it is possible to observe a
 340 shoulder that can be attributed to a simultaneous excitation of two
 341 electrons: next to the 1s core electron, also a t_2 valence electron is
 342 promoted to a t_2^* unoccupied orbital.⁴⁶

343 Another important parameter that provides information about
 344 the valence state of Cr from XANES spectra is the shift of the
 345 absorption edge position. In general, a shift toward higher energies is
 346 observed when there is an increase in the valency of the absorbing
 347 atom and/or of the electronegativity of the nearest neighbor atoms.
 348 A recent study on different chromium complexes⁴⁷ has demon-
 349 strated the strong dependence of the shift of the absorption edge
 350 energy on the ligand geometry but also highlighted the impossibility
 351 to accurately determine oxidation states of unknown complexes by
 352 simply scaling their edge positions. As shown for Cr(VI) reference
 353 compounds (Figure 1A, spectra 03, 06, 08, 13), a shift of the
 354 absorption edge toward lower energy may be correlated to an
 355 increase of the degree of polymerization of the chromate moieties.⁴⁸

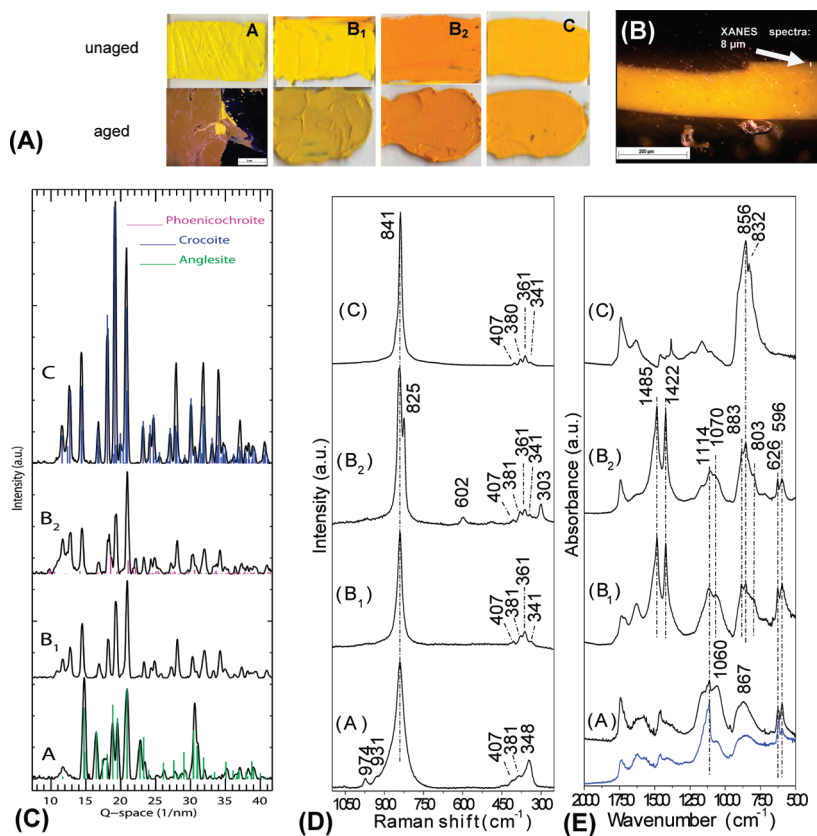


Figure 2. Panel A: Images of model samples A, B₁, B₂, and C before (on top) and after (below) aging process (800 h). Panel B: Visible light microscopy image of model sample A. The line along which Cr K-edge XANES spectra were acquired is indicated (see Figure 3C). Panels C–E: SR μ -XRD, μ -Raman, and FTIR results for unaged model samples A, B₁, B₂, and C. In blue line: FTIR spectrum of aged sample A (see text for details).

Artificially Aged Model Samples. In order to induce the darkening of chrome yellow under the influence of light and heat, several model paint samples were prepared and artificially aged in identical conditions. Prior to SR μ -XANES and μ -XRF analysis, a characterization of these model samples before and after aging was performed by means of different techniques, and the results are summarized in Table 1.

Optical and Microscopic Observations. Figure 2A shows the visual aspect of the oil paint model samples before and after aging. The formation of a thin brown layer on the outer surface of sample A is clearly visible, similar to that observed by Cole,¹⁰ who described the alteration process as superficial and attributed it to a defective lattice structure, indicating that other factors, such as dimension of the pigment particles and the method of preparation, can have a significant effect on the light-fastness of PbCrO₄. Although in all model samples to some extent a darkening of the visual aspect can be observed, the other model samples do not show the same profound discoloration as does sample A.

SR μ -XRD, μ -Raman, and FTIR Analyses. In general, no significant difference in the XRD, μ -Raman, or transmission FTIR spectra were observed between the unaged and the aged model samples. Hence, Figure 2C–E only show the results obtained prior to the aging process. This fact is attributed to the limited thickness of the alteration layer and to the fact that only μ -XRD measurements in transmission mode were performed. Also, in a mixture of Cr(VI)- and Cr(III)-species, the high Raman scattering power of chromates makes it difficult to detect Cr(III) compounds. While linseed oil was present as organic binder in all model samples, XRD, μ -Raman, and transmission FTIR

analyses did show a marked difference between the inorganic composition of sample A and the other model samples. μ -XRD measurements revealed crystalline lead chromate (crocoite, PbCrO₄) in all model samples except A, of which the diffraction pattern (Figure 2C) only reveals the presence of lead sulfate (anglesite, PbSO₄). A second, red-colored lead chromate pigment, called phoenicochroite [Pb₂O(CrO₄)], was mixed with crocoite in sample B₂ in order to obtain an orange paint. μ -Raman analyses (Figure 2D) confirm the presence of crocoite in all paint samples, as characterized by a strong band at 841 cm⁻¹ (CrO₄²⁻ symmetric stretching) and several bands of medium intensity at 407, 381, and 361 cm⁻¹ (CrO₄²⁻ bending modes).⁴⁹ In the Raman spectra of sample A, some differences in the shape of the bands located between 410 and 350 cm⁻¹ were observed, characterized by a signal of medium intensity at 349 cm⁻¹ that is not present in the spectra of the other model samples. In addition, the band at 974 cm⁻¹ (SO₄²⁻ symmetric stretching)⁵⁰ revealed the presence of lead sulfate. In agreement to μ -XRD, Raman measurements on sample B₂ showed the presence of phoenicochroite, characterized by an additional band at 825 cm⁻¹ (CrO₄²⁻ stretching).⁴⁹ Two signals at 303 and 602 cm⁻¹ are attributed to cadmium yellow (CdS),⁵¹ likely present as an impurity of the pigment. FTIR measurements (Figure 2E) revealed the presence of lead sulfate on all samples except C, as demonstrated by the signals around 1100 and 1000 cm⁻¹ (SO₄²⁻ asymmetric stretching) and the bands at 626 and 596 cm⁻¹ (SO₄²⁻ asymmetric bending).⁵⁰ This compound is less abundantly present in samples B₁ and B₂ than in A. In all samples, the presence of lead chromate is confirmed by the signals located between 900 and 800 cm⁻¹ (CrO₄²⁻ asymmetric

385
386
387
388
389
390
391
392
393
394
395
396
397
398
399
400
401
402
403
404
405
406
407
408
409
410
411
412
413

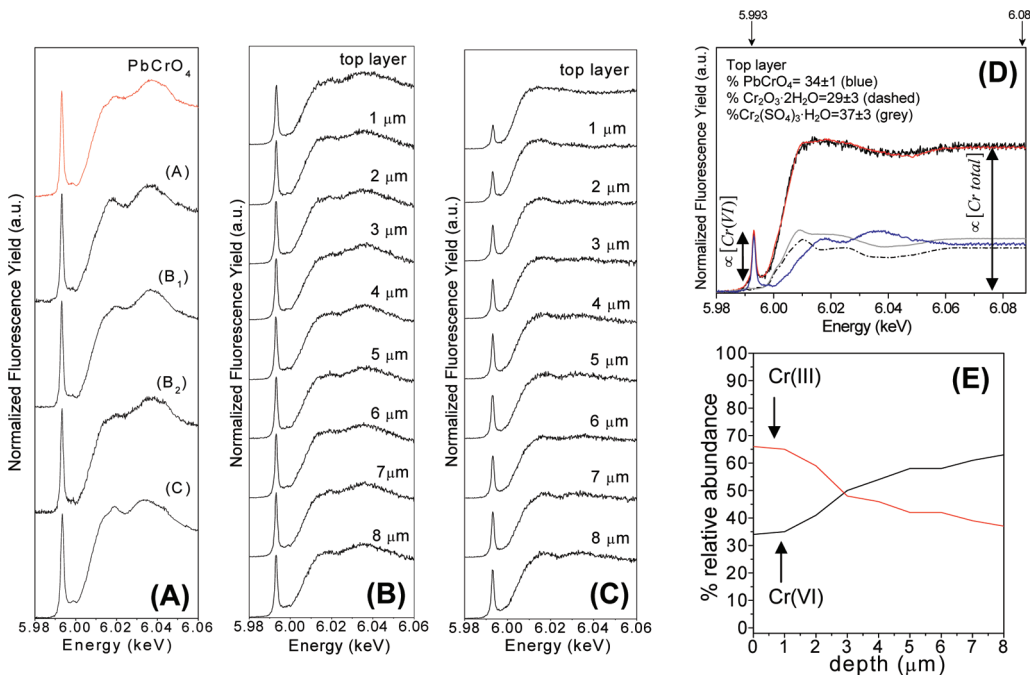


Figure 3. Panel A: Cr K-edge XANES spectra of unaged model samples. Comparison between the PbCrO₄ reference (red) and model samples A, B₁, B₂, and C. Panels B and C: series of Cr K-edge XANES spectra recorded from aged and cross-sectioned model samples of B₂ (Panel B) and A (Panel C). The XANES spectra were recorded with an increment of 1 μm, moving from surface (exposed layer) toward the underlying bulk material along a line perpendicular to the surface. In the case of sample A, this line is indicated in Figure 2B. Panels D and E: quantitative estimation of the related abundance of Cr(III) and Cr(VI) compounds vs depth in aged sample A. Panel D: Fitting of the μ -XANES spectra as a linear combination of reference spectra. (Red) Fit of the experimental data (black) by combination of PbCrO₄ (blue), Cr₂O₃·2H₂O (dashed), and Cr₂(SO₄)₃·H₂O (gray) and estimation of their relative abundances. Panel E: Percentage of the relative abundances of Cr(VI) (black) and Cr(III) (red) vs depth.

stretching).⁴⁹ Both in the Raman and FTIR spectra, the differences in the shape of the bands assigned to sulfates and chromates are attributed to the different ratio between these two isostructural anions and their arrangement inside the pigment lattice.^{52,53} Additionally in samples B₁ and B₂, the presence of a hydrated carbonate compound (likely magnesium carbonate) is suggested by signals at 3650 (free –OH stretching, not shown) and 1485 and 1422 cm^{–1} (CO₃^{2–} asymmetric stretching).⁵⁴ After aging, only the FTIR spectrum of aged sample A (blue line) features minor differences relative to the spectrum of unaged sample (black line), as illustrated in Figure 2E: a decrement of the signal at 1060 cm^{–1} and an inversion in the intensity of the bands located at 626 and 596 cm^{–1} are observed.

Considering that nevertheless a significant discoloration of sample A has taken place, regarding the model samples, most analytical efforts employing micro-X-ray techniques and EELS were focused on this material.

Local Cr-Speciation Measurements. Figure 3A demonstrates that the XANES spectra recorded on all unaged model samples are similar to that of the pure PbCrO₄ reference. Several measurements performed on the aged B₁, B₂, and C samples, either at the outer layer or at unexposed material underneath the surface did not reveal any difference. As an example, Figure 3B shows a series of XANES spectra collected from a cross-section of aged sample B₂ obtained along a line perpendicular to the exposed surface.

Similar measurements performed on aged sample A, however, show a significant difference between the discolored surface and the yellow material immediately below (Figure 3C). Since the XANES spectra from the surface show a clear decrease of the intensity of the Cr pre-edge peak at 5.993 keV and feature a shift of the absorption edge toward lower energies, a substantial

reduction of the original Cr(VI) has taken place at the surface. However, also on the still-yellow areas of the material, the reduction of Cr is observed, albeit to a lesser degree than at the surface. In order to extract semiquantitative data on the abundance of Cr(III)- and Cr(VI)-species vs depth from the spectra in Figure 3C, each normalized spectrum was fitted as a linear combination of the XANES spectra of pure lead chromate (PbCrO₄), viridian (Cr₂O₃·2H₂O), and chromium sulfate hydrate [Cr₂(SO₄)₃·H₂O]; the “best fit” weighting coefficients of the different species were calculated by using the ATHENA software.⁴² This combination of reference compounds yields the best fit (see Figure 3D for an example) while it is in part compatible with the observations during the precharacterization phase and the results obtained by means of EELS at higher magnification (see below). Indeed, in the presence of abundant sulfates (present as anglesite), upon formation of Cr(III) ions, it is not implausible that Cr₂(SO₄)₃·H₂O is formed as a secondary reaction product. Figure 3D and 3E summarize the fitting results using the PbCrO₄/Cr₂O₃·2H₂O/ Cr₂(SO₄)₃·H₂O model. Nevertheless, considering the complexity of the painting matrix, the possible presence of organo-Cr(III) compounds should not be excluded. Although of lower quality (particularly when the postedge region is more structured), good fitting results were also obtained using chromium(III) acetate hydroxide [(CH₃COO)₇Cr₃(OH)₂] instead of Cr₂(SO₄)₃·H₂O as part of the fitting model; acetate ions may be included or absorbed on PbCrO₄ during the procedure preparation,¹⁰ or formed in situ by degradation of the organic binder. Since Cr(III) acetate and sulfate have similar XANES spectra (see Figure 1B), both fitting models yield similar Cr(III):Cr(VI) ratios and convey the same message.

It is noteworthy that three fitting components [either $\text{Cr}_2(\text{SO}_4)_3 \cdot \text{H}_2\text{O}$ or $(\text{CH}_3\text{COO})_7\text{Cr}_3(\text{OH})_2$, $\text{Cr}_2\text{O}_3 \cdot 2\text{H}_2\text{O}$, and PbCrO_4] are required for a good description of the XANES spectra recorded along the first 3 μm below the brown layer, while only two components ($\text{Cr}_2\text{O}_3 \cdot 2\text{H}_2\text{O}$ and PbCrO_4) are required to fit the spectra recorded from 5 to 8 μm below the surface. As shown in Figure 3E, the Cr(VI) concentration, expressed as $[\text{Cr(VI)}]/[\sum \text{Cr}]$, decreases progressively from the yellow bulk of the sample (where it is present at the level of 50–60%) toward the exposed, brown surface (where it reaches a value of around 30–40%). Clearly a positive correlation between the darkening and the Cr(III) abundance can be observed here (Figure 3E); a fairly thin alteration layer of ca. 2–3 μm thickness is observed, also confirmed by other measurements (see below). This thickness is similar to that observed by Casadio et al.³⁵ on altered $\text{K}_2\text{O} \cdot 4\text{ZnCrO}_4 \cdot 3\text{H}_2\text{O}$ samples. However, in contrast to their conclusions, the present XANES data do not reveal any indications about the presence of dichromate compounds. In case XANES reference spectra of dichromatic species (see Figure 1A, spectra 03, 06, and 08) are included in the fitting model, a fit of reduced quality is obtained. We also do not observe the slight broadening of the Cr–K pre-edge peak that is visible in the dichromate reference spectra of Figure 1A.

The formation of a hydrated version of the degradation species $\text{Cr}_2\text{O}_3 \cdot 2\text{H}_2\text{O}$ is understandable in view of the fact that (a) it was demonstrated by FTIR analyses, specifically by the presence of the stretching (around 3450 cm^{-1} , not shown) and bending mode (1620 cm^{-1}) bands of the OH group, that water is present in both the unaged and aged versions of sample A and (b) the aging process took place in an atmosphere having 50% RH while the aging temperature, kept between 50 and 60 °C, was not sufficiently high to drive off all the water present inside the sample.

EELS Measurements. In order to establish whether or not the brown alteration layer was a homogeneous mixture of compounds, a thin cross-section of the upper 2 μm of the brown alteration layer of sample A was prepared by FIB, and STEM/EELS measurements at the Cr L_{2,3}- and O K-edges were performed. Figure 4 summarizes some of the results obtained. In Figure 4A an overview picture of the cross-section is shown; the photograph depicts the upper 1 × 1.4 μm^2 of the alteration layer. In a C-rich matrix (light areas of the photograph) different types of grains with diameters between 10 and 150 nm are present. About half of the grains are rich in Pb and S and feature the crystalline structure of anglesite (PbSO_4). Some of these particles are coated with a Cr(III)-containing layer (Figure 4C).

In Figure 4B, EELS O-K and Cr-L_{2,3} spectra of some reference compounds are shown. The spectrum of $\text{Cr}_2\text{O}_3 \cdot 2\text{H}_2\text{O}$ features a symmetric Cr-L₃ peak near 578 eV while for the PbCrO_4 compound this peak is close to 582 eV (see thick dashed line in Figure 4D). On the other hand, the O-K EELS spectrum of PbSO_4 distinguishes itself from that of $\text{Cr}_2\text{O}_3 \cdot 2\text{H}_2\text{O}$ and PbCrO_4 by the presence of a sharp feature at an energy-loss value of ca. 538 eV (thin dashed line in Figure 4D). These characteristic features are also visible in the EELS line scan shown in Figure 4D that was taken along the vertical axis of the area shown in Figure 4A by averaging horizontally the EELS signals obtained at different vertical coordinates. In this line scan, close to/just below the surface the averaged EELS spectra resemble closely that of PbSO_4 (thin dashed line) while deeper in the bulk, the average spectrum starts to look more like that of PbCrO_4 (thick dashed line in Figure 4D). In between and at the very

surface, spectra in which the $\text{Cr}_2\text{O}_3 \cdot 2\text{H}_2\text{O}$ character dominates are also apparent.

By exploiting the spectral features indicated with the dashed lines and more specifically by selecting energy windows in the regions of 532–534 eV and 538–540 eV in the EELS spectra, it is possible to visualize the distribution of $\text{Cr}_2\text{O}_3 \cdot 2\text{H}_2\text{O}$ and PbSO_4 on the nanoscale throughout the examined area. These maps, detailed in Figure 4C, reveal that the Cr_2O_3 phase is present as a (newly formed) precipitation coating on the anglesite particles.

Chemical State Mapping. In order to visualize the distribution of Cr(VI)- and Cr(III)-species vs depth in aged sample A and to compare to the results obtained from the linear combination fitting of the XANES spectra, μ -XRF maps of the same area were recorded at two different excitation energies: i.e., (a) at 5.993 keV, favoring the excitation of the Cr(VI)-species; (b) at 6.086 keV to obtain a Cr–K_α fluorescence intensity map that is proportional to the total Cr content at a given position (i.e., irrespective of its oxidation state). The resulting Pb and Cr μ -XRF maps (not shown) demonstrate that these elements appear as main constituents and that they are both homogeneously distributed.

The following simple semiquantitative image processing method was employed to convert the two Cr–K_α intensity maps into Cr(III) and Cr(VI) abundance distributions. In performing these calculations, we implicitly assume that the total amount of Cr present at any position in the map is either present as (a) one or more Cr(VI) compounds, all having XANES spectra very similar to that of PbCrO_4 or as (b) one or more Cr(III) compounds, all having XANES spectra very similar to that of $\text{Cr}_2\text{O}_3 \cdot 2\text{H}_2\text{O}$, $\text{Cr}_2(\text{SO}_4)_3 \cdot \text{H}_2\text{O}$, and/or $(\text{CH}_3\text{COO})_7\text{Cr}_3(\text{OH})_2$. Under this assumption, and considering that at $E_0 = 5.993$ keV (the Cr pre-edge energy), there is a negligible contribution to the Cr–K_α fluorescence from Cr(III) compounds (Figure 1B), the percentage concentration of Cr(VI) in every pixel (x,y) of the images is equal to the scaled relative intensity of both images at this location:

$$c_{\text{Cr(VI)}}(x,y) (\%) = \frac{I_{E_0=5.993\text{keV}}^{\text{Cr}}(x,y)/I_{E_0=5.993\text{keV}}^{\text{Cr}, \text{PbCrO}_4}}{I_{E_0=6.086\text{keV}}^{\text{Cr}}(x,y)/I_{E_0=6.086\text{keV}}^{\text{Cr}, \text{PbCrO}_4}} \times 100\%$$

while the local concentration of Cr(III) compounds is equal to:

$$c_{\text{Cr(III)}} (\%) = 100\% - c_{\text{Cr(VI)}} (\%)$$

The scaling ratio ($I_{E_0=5.993\text{keV}}^{\text{Cr}, \text{PbCrO}_4}/(I_{E_0=6.086\text{keV}}^{\text{Cr}, \text{PbCrO}_4})$) is derived from the intensity readings of the XANES spectrum of the PbCrO_4 standard (Figure 1A, spectrum 01) and is equal to a value of 1.2.

Figure 5A and 5B shows the $c_{\text{Cr(VI)}}$ and $c_{\text{Cr(III)}}$ maps derived in this manner from a polished cross-section of aged sample A. In good agreement with the data obtained from the linear combination fitting of XANES spectra (Figure 3E), Cr(III)-species are observed to be enriched in the superficial layer; this contains up to 60–70% of Cr(III). Because the Cr-speciation only gradually changes (see also Figure 3E), it is not possible to assign a very precise value to the layer thickness. In general, we observed alteration layer thicknesses between 1 and 3 μm .

Cr(III)-Species and the Dark-Brown Color of the Alteration Layer. On first sight, the green Cr(III) compound $\text{Cr}_2\text{O}_3 \cdot 2\text{H}_2\text{O}$ (the green pigment viridian) is not able to explain the dark-brown color of the superficial alteration layer. Nevertheless, it must be realized that the observation of reduced Cr-species implies that other components of the paint, organic and/or inorganic in nature, have played the role of electron-donors and

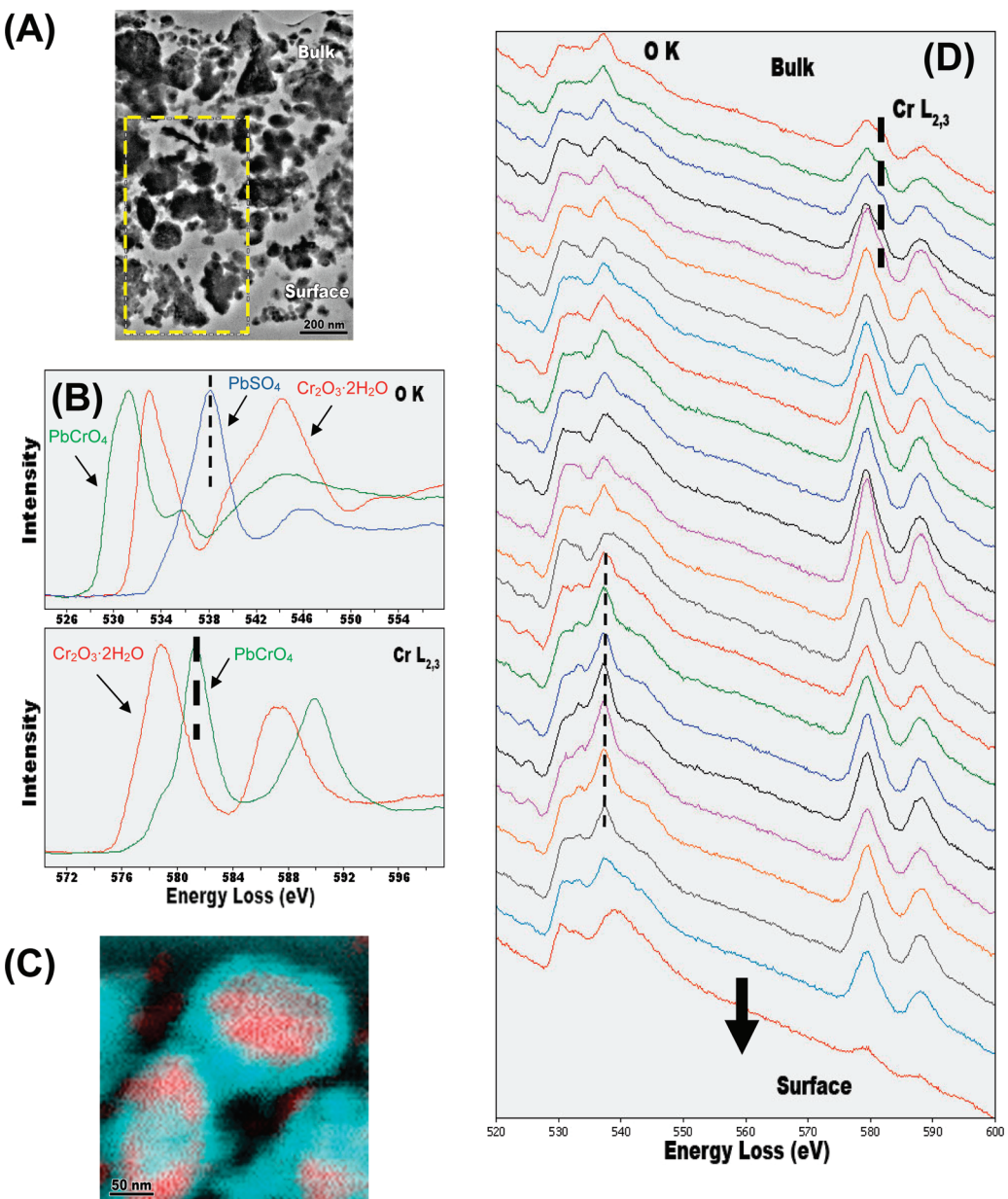


Figure 4. STEM/EELS data obtained from the brown alteration layer of sample A. Panel A: Overview STEM picture ($1 \times 1.4 \mu\text{m}^2$) of FIB cross-section. Panel B: EELS O K-edge and Cr L_{2,3}-edge reference spectra of (red) Cr₂O₃·2H₂O, (blue) PbSO₄, (green) PbCrO₄. Panel C: high-resolution RG composite map of different compounds coating an anglesite (PbSO₄) particle (red: PbSO₄, cyan: Cr₂O₃·2H₂O). Panel D: EELS line scan (a.u.), composed of spectra collected in the area indicated in Figure 4A in the direction of the arrow; spacing of spectra: 40 nm. Arrow indicates scan direction.

therefore have become oxidized. In general, the following factors may contribute additionally to the observed color:

- 594 (a) The presence of (polynuclear) Cr(III) compounds such
595 as Cr(III) acetates or sulfates, of which the color can vary
596 from green, gray-green, violet, to blue-violet.⁵⁵
- 597 (b) The partial degradation of the organic binding medium of
598 the paint.
- 599 (c) The possible formation of other inorganic degradation
600 products, such as PbO₂ and PbS (both black).

601 To establish whether or not the formation of the brown
602 alteration color is reproducible, a series of additional model
603 samples were prepared by mixing linseed oil and several synthesized
604 powders of coprecipitates of different PbCrO₄:PbSO₄
605 ratios. The recently executed aging of these model samples

(50% relative humidity, UV-visible irradiation) leads to a clear and reproducible darkening of the oil paint samples that is particularly significant for those containing larger amounts of sulfate (PbSO₄:PbCrO₄ ≥ 1). The formation of a superficial brown-green layer is clearly visible, similar to that observed on aged model sample A. In contrast to the experiments conducted by Casadio et al.,³⁵ the presence of SO₂ was not required to promote the alteration; possibly the sulfates present inside the PbCrO₄:PbSO₄ mixtures play a role similar to that of SO₂.

606 **Cr-Speciation in Original Paint Samples from Paintings of
607 Vincent van Gogh and the Role of Sulfur Species on Cr(VI)
608 Reduction.** To establish whether or not the above-described
609 reduction phenomenon effectively takes place in real situations,
610 μ -XANES and μ -XRF spectrometry were employed to study two

611
612
613
614
615
616
617
618
619
620
621

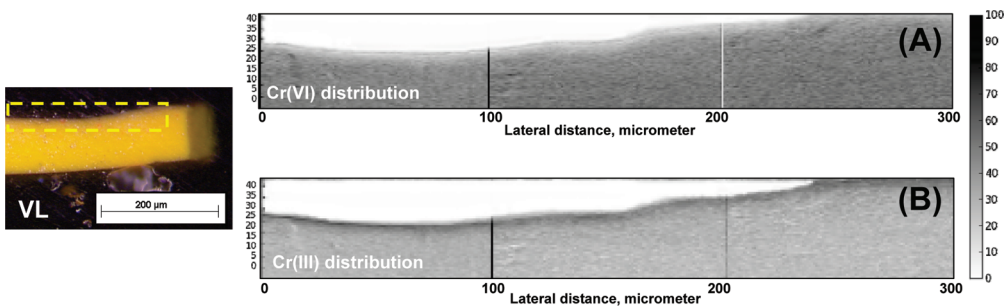


Figure 5. Cr chemical state maps of aged sample A. (Left panel) Visible light microscopy image (VL) of embedded aged model sample and (right panels) species-specific distribution in the indicated area of (A) Cr(VI) and (B) Cr(III) maps obtained by μ -XRF scanning at 5.993 and 6.086 keV. The two maps demonstrate that the brown layer on the top is dominated by one or more Cr(III) compounds (60–70% of \sum Cr); in the underlying yellow layer, these are present but at lower concentration. Map size: $42 \times 300 \mu\text{m}^2$, pixel size: $0.25 \times 1 \mu\text{m}^2$, dwell time: 0.1 s.

622 embedded paint cross-sections taken from paintings by Vincent
623 van Gogh from the collection of the Van Gogh Museum (VGM),
624 Amsterdam. In these paintings, alteration of the chrome yellow
625 paint was apparent. As described in more detail in the Part 2 of
626 this study, this is effectively the case.⁵⁶ Consistent with the
627 observations made on the model samples, the Cr-reduction
628 appears to take place only in areas that are rich in sulfates. On
629 the basis of this information, it was possible to formulate a
630 hypothesis regarding the alteration mechanism taking place.
631

At this instance, however, considering the above-described
632 results and those of Casadio et al.,³⁵ in which SO_2 was shown to
633 be one of the agents promoting the alteration process of zinc
634 potassium chromate pigments, we limit ourselves to concluding
635 that sulfur species (i.e., sulfates or perhaps more reduced forms
636 of S) appear to play a key role in the mechanism of chrome
637 yellow degradation.

CONCLUSIONS

The darkening of chrome yellow is a complex alteration
638 problem that affects specific paintings from the end of 19th
639 Century. In the first part of the present work, a combination of
640 synchrotron radiation-based X-ray techniques, such as μ -XRF,
641 μ -XANES, and EELS, and more conventional spectroscopic
642 methods was employed to investigate artificially aged model
643 samples. This allowed us to elucidate part of the degradation
644 mechanism of chrome yellow.

Our observations indicate that the alteration of yellow
645 PbCrO_4 is caused by reduction of the original Cr(VI) to Cr(III).
646 Sulfates appear to play an essential role in promoting this
647 reduction process. Only in model samples rich in lead sulfate
648 and in which the lead chromate is present in a very fine-grained/
649 amorphous form was the formation of a superficial brown
650 colored layer (of $1\text{--}3 \mu\text{m}$ thickness) observed after an artificial
651 aging process involving UV irradiation. The presence of SO_2 was
652 not required to promote the alteration.

By means of both μ -XANES and EELS, the alteration layer was
653 shown to contain significant amounts (up to 60%) of Cr(III).
654 Investigations at the nanoscopic level revealed that $\text{Cr}_2\text{O}_3 \cdot 2\text{H}_2\text{O}$
655 has formed at the surface of the original yellow paint. This phase
656 is formed as an external coating on submicroscopic anglesite
657 grains present in the paint. Using a combination of PbCrO_4 ,
658 $\text{Cr}_2\text{O}_3 \cdot 2\text{H}_2\text{O}$, and either $\text{Cr}_2(\text{SO}_4)_3 \cdot \text{H}_2\text{O}$ or $(\text{CH}_3\text{COO})_7\text{Cr}_3 \cdot (\text{OH})_2$, the Cr K-edge XANES spectra recorded from the altered
659 model samples can be satisfactorily described, indicating that in
660 the altered layer, Cr is roughly equally distributed over the three
661 above-mentioned Cr-species. No indications of the presence of
662

Cr(VI) dichromate ions were observed. The brown color of the
663 alteration layer is attributed to either the oxidation of the binding
664 medium, the presence of polynuclear Cr(III)-species, or a
665 combination of both. To demonstrate that the chrome yellow
666 alteration phenomena observed in the aged model samples also
667 takes place in real paintings, the second part of this work focuses
668 on the study of microsamples from paintings by Vincent van Gogh.

AUTHOR INFORMATION

Corresponding Author

*Phone: +32 3 820 2373. Fax: +32 3 820 23 76. E-mail: koen.janssens@ua.ac.be.

ACKNOWLEDGMENT

This research was funded by grants from ESRF (experiment
679 EC-504) and by HASYLAB (experiments II-20080130 EC and
680 II-20070157 EC) and was supported by the Interuniversity
681 Attraction Poles Programme - Belgian Science Policy (IUAP
682 VI/16). The text also presents results of GOA "XANES meets
683 ELNES" (Research Fund University of Antwerp, Belgium) and
684 from FWO (Brussels, Belgium) projects nos. G.0103.04,
685 G.0689.06, and G.0704.08. The staff of the Van Gogh Museum,
686 Amsterdam, is acknowledged for their agreeable cooperation. We
687 also thank Nathalie Lacquie of the Royal Academy of Fine Arts
688 of Antwerp for her help with the aging of the model samples.
689 L.M. was financially supported by the Erasmus Placement in the
690 framework of Lifelong Learning Programme (A.Y. 2009-2010).
691 The EU Community's FP7 Research Infrastructures program
692 under the CHARISMA Project (Grant Agreement 228330) is
693 also acknowledged.

REFERENCES

- (1) Hendriks, E. In *New Views on Van Gogh's Development in Antwerp en Paris: An Integrated Art Historical and Technical Study of His Paintings in the Van Gogh Museum*; Hendriks, E., Van Tilborgh, L., Eds.; University of Amsterdam: Amsterdam, The Netherlands, 2006; pp 149–150.
- (2) Kirby, J.; Stonor, K.; Roy, A.; Burnstock, A.; Grout, R.; White, R. *Natl. Gallery Tech. Bull.* **2003**, 28, 4–37.
- (3) Townsend, J. H. *Stud. Conserv.* **1993**, 38, 231–254.
- (4) Cove, S. In *Constable*; Parris, L.; Fleming-Williams, I., Eds.; Tate
Gallery: London, 1991; pp 493–518.
- (5) Butler, M. H. *Bull. Am. Inst. Conserv. Historic Artistic Works* **1973**, 13, 77–85.
- (6) Bomford, D.; Kirby, J.; Leighton, J.; Roy, A. *Art in the Making: Impressionism*; London: National Gallery Publications, 1990; p 158.

- (7) Van der Snickt, G.; Janssens, K.; Schalm, O.; Aibéo, C.; Kloust, H.; Alfeld, M. *X-Ray Spectrom.* **2010**, *39*, 103–111.
- (8) Kühn, H.; Curran, M. In *Artists' Pigments: a handbook of their history and characteristics*; Feller, R. L., Ed.; Cambridge University Press, 1986; Vol. 1, pp 187–200.
- (9) Eastaugh, N.; Walsh, V.; Chaplin, T.; Siddall, R. *The Pigment Compendium [CD-ROM]*; Elsevier: New York, 2004.
- (10) Cole, R. J. *Paint Res. Assoc. Tech. Pap.* **1955**, *199*, 1–62.
- (11) Watson, V.; Clay, H. F. J. *Oil Colour Chem. Assoc.* **1955**, *38*, 167–177.
- (12) Cowley, A. C. D. *Rev. Prog. Coloration* **1986**, *16*, 16–23.
- (13) Bronwyn, L.; Burnstock, A.; Jones, C.; Hallebeek, P.; Boon, J. J.; Keune, K. In *Preprints of the 14th Triennial Meeting of ICOM Committee for Conservation*, The Hague, September 12–16, 2005; James & James: London, 2005, Vol. 2, pp 803–813.
- (14) Van der Snickt, G.; Dik, J.; Cotte, M.; Janssens, K.; Jaroszewicz, J.; De Nolf, W.; Groenewegen, J.; Van der Loeff, L. *Anal. Chem.* **2009**, *7*, 2600–2610.
- (15) Paillet De Montabert, J. N. *Traité complet de la Peinture*; Bossange père: Paris, 1829, p 221.
- (16) Eibner, A. *Chem. Ztg.* **1911**, *82*, 753–755.
- (17) Haug, R. *Dtsch. Farben-Z.* **1951**, *5*, 343–348.
- (18) Erkens, L. J. H.; Hamers, H.; Hermans, R. J. M.; Claeys, E.; Bijnens, M. *Surface Coat. Int., Part B* **2001**, *84*, 1969–1976.
- (19) Somme-Dubru, M. L.; Genet, M.; Mathieu, A.; Rouxhet, P. G.; Rodrique, L. *J. Coat. Technol.* **1981**, *53*, 51–56.
- (20) Lashof, T. W. *J. Chem. Phys.* **1943**, *11*, 196–202.
- (21) Bloch, G. *Double—Liaison* **1969**, *161*, 51–60.
- (22) Loyaux-Lawniczak, S.; Refait, P.; Lecomte, P.; Ehrhardt, J. J.; Génin, J. M. R. *Hydrol. Earth Syst. Sci.* **1999**, *3*, 593–599.
- (23) Abdel-Samad, H.; Watson, P. R. *Appl. Surf. Sci.* **1997**, *108*, 371–377.
- (24) Boursiquot, S.; Mullet, M.; Ehrhardt, J. J. *Surf. Interface Anal.* **2002**, *34*, 293–297.
- (25) Kim, C.; Zhou, Q.; Deng, B.; Thornton, E. C.; Xu, H. *Environ. Sci. Technol.* **2001**, *35*, 2219–2225.
- (26) Mytych, P.; Ciésla, P.; Stasicka, Z. *Int. J. Photoenergy* **2001**, *3*, 181–186.
- (27) Tzou, Y. M.; Loepert, R. H.; Wang, M. *J. Environ. Qual.* **2003**, *32*, 2076–2084.
- (28) Navio, J. A.; Colòn, G.; Trillas, M.; Peral, J.; Domènech, X.; Testac, J. J.; Padròn, J.; Rodrguez, D.; Litterc, M. I. *Appl. Catal. B: Environmental* **1998**, *16*, 187–196.
- (29) Khalil, B.; Mourad, W. E.; Rophael, M. W. *Appl. Catal. B* **1998**, *17*, 267–273.
- (30) Ku, Y.; Jung, I. L. *Water Res.* **2001**, *1*, 135–142.
- (31) Perez-Benito, F.; Arias, C. *J. Phys. Chem. A* **1997**, *101*, 4726–4733.
- (32) van Niekerk, W.; Pienaar, J. J.; Lachmann, G.; van Eldik, R.; Hamza, M. *Water SA* **2007**, *33*, 619–626.
- (33) Burnstock, A. R.; Jones, C. G.; Cressey, G. Z. *Kunsttechnol. Konserv.* **2003**, *17*, 74–84.
- (34) Casadio, F.; Gray, K. A.; Warta, R.; Fiedler, I. In *Preprints of the 15th Triennial Meeting of ICOM Committee for Conservation*, New Delhi, September 22–26, 2008; Allied Publishers Pvt Ltd, 2008, Vol. 2, pp 642–650.
- (35) Casadio, F.; Xie, S.; Rukes, S. C.; Myers, B.; Gray, K. A.; Warta, R.; Fiedler, I. *Anal. Bioanal. Chem.* **2010**, DOI: 10.1007/s00216-010-4264-9.
- (36) Cotte, M.; Susini, J.; Sole, V. A.; Taniguchi, Y.; Chillida, J.; Checroun, E.; Walter, P. *J. Anal. At. Spectrom.* **2008**, *23*, 820–828.
- (37) Lluveras, A.; Boulanand, S.; Roque, J.; Cotte, M.; Giraldez, P.; Vendrell-Saz, M. *Appl. Phys. A: Mater. Sci. Process.* **2008**, *90*, 23–33.
- (38) Salvadó, N.; But, S.; Nicholson, J.; Emerich, H.; Labrador, A.; Pradell, T. *Talanta* **2009**, *79*, 419–428.
- (39) De Nolf, W.; Jaroszewicz, J.; Terzano, R.; Lind, O. C.; Salbu, B.; Vekemans, B.; Janssens, K.; Falkenberg, G. *Spectrochim. Acta, Part B* **2009**, *64*, 775–781.
- (40) Cotte, M.; Welcomme, E.; Solé, V. A.; Salomé, M.; Menu, M.; Walter, P.; Susini, J. *Anal. Chem.* **2007**, *79*, 6988–6994.
- (41) Susini, J.; Salomé, M.; Fayard, B.; Ortega, R.; Kaulich, B. *Surf. Rev. Lett.* **2002**, *9*, 203–211.
- (42) Solé, V. A.; Papillon, E.; Cotte, M.; Walter, P.; Susini, J. *Spectrochim. Acta, Part B* **2007**, *62*, 63–68.
- (43) Ravel, B.; Newville, M. *J. Synchrotron Radiat.* **2005**, *12*, 537–541.
- (44) Peterson, M. L.; Brown, G. E.; Parks, G. A.; Stein, C. L. *Geochim. Cosmochim. Acta* **1997**, *61*, 3399–3412.
- (45) Pantelouris, A.; Modrow, H.; Pantelouris, M.; Hormes, J.; Reinen, D. *Chem. Phys.* **2004**, *300*, 13–22.
- (46) Bianconi, A.; Garcia, J.; Benfatto, M.; Marcelli, A.; Natoli, C. R.; Ruiz-Lopez, M. F. *Phys. Rev. B* **1991**, *43*, 6885–6892.
- (47) Tromp, M.; Moulin, J.; Reid, G.; Evans, J. In *AIP Conference Proceedings: 13th International Conference on X-ray Absorption Fine Structure-XAFS13*, Stanford, California, July 9–14, 2006; Hedman, B.; Pianetta, P., Eds.; 2007, Vol. 882; pp 699–701.
- (48) Farges, F. *Phys. Chem. Miner.* **2009**, *36*, 463–481.
- (49) Frost, R. L. *J. Raman Spectrosc.* **2004**, *35*, 153–158.
- (50) Lane, M. D. *Am. Mineral.* **2007**, *92*, 1–18.
- (51) Bell, I. M.; Clark, R. J. H.; Gibbs, P. *J. Spectrochim. Acta, Part A* **1997**, *53*, 2159–2179.
- (52) Stoilova, D.; Georgiev, M.; Marinova, D. *J. Mol. Struct.* **2005**, *738*, 211–215.
- (53) Alía, J. M.; Edwards, H. G. M.; Fernández, A.; Prieto, M. *J. Raman Spectrosc.* **1999**, *30*, 105–114.
- (54) Zhang, Z.; Zheng, Y.; Ni, Y.; Liu, Z.; Chen, J.; Liaug, X. *J. Phys. Chem. B* **2006**, *110*, 12969–12973.
- (55) Vinokurov, E. G.; Kuznetsov, V. V.; Bondar, V. V. *Russian J. Coord. Chem.* **2004**, No. 30, 496–504.
- (56) Monico, L.; Van der Snickt, G.; Janssens, K.; De Nolf, W.; Miliani, C.; Dik, J.; Radepont, M.; Hendriks, E.; Geldof, M.; Cotte, M. *Anal. Chem.* **2010**, DOI:10.1021/ac1025122.